University of Nebraska - Lincoln
DigitalCommons@University of Nebraska - Lincoln

US Department of Energy Publications | U.S. Department of Energy

2002

Modeling the Inhibition of the Bacterial Reduction of U(VI) by β-MnO2(s)

Chongxuan Liu
Pacific Northwest National Laboratory, chongxuan.liu@pnl.gov

John M. Zachara
Pacific Northwest National Laboratory, john.zachara@pnl.gov

James K. Fredrickson
Pacific Northwest National Laboratory, jim.fredrickson@pnl.gov

David W. Kennedy
Pacific Northwest National Laboratory

Alice Dohnalkova
Pacific Northwest National Laboratory

Follow this and additional works at: https://digitalcommons.unl.edu/usdoepub

 Part of the Bioresource and Agricultural Engineering Commons

Liu, Chongxuan; Zachara, John M.; Fredrickson, James K.; Kennedy, David W.; and Dohnalkova, Alice, "Modeling the Inhibition of the Bacterial Reduction of U(VI) by β-MnO2(s)" (2002). *US Department of Energy Publications*. 221.
https://digitalcommons.unl.edu/usdoepub/221

This Article is brought to you for free and open access by the U.S. Department of Energy at DigitalCommons@University of Nebraska - Lincoln. It has been accepted for inclusion in US Department of Energy Publications by an authorized administrator of DigitalCommons@University of Nebraska - Lincoln.

Environ. Sci. Technol. **2002**, *36,* 1452−1459

Modeling the Inhibition of the Bacterial Reduction of U(VI) by β-$MnO_{2(s)}$

CHONGXUAN LIU,* JOHN M. ZACHARA, JAMES K. FREDRICKSON, DAVID W. KENNEDY, AND ALICE DOHNALKOVA

Pacific Northwest National Laboratory, Richland, Washington 99352

Pyrolusite (β-$MnO_{2(s)}$) was used to assess the influence of a competitive electron acceptor on the kinetics of reduction of aqueous uranyl carbonate by a dissimilatory metal-reducing bacterium (DMRB), *Shewanella putrefaciens* strain CN32. The enzymatic reduction of U(VI) and β-$MnO_{2(s)}$ and the abiotic redox reaction between β-$MnO_{2(s)}$ and biogenic uraninite ($UO_{2(s)}$) were independently investigated to allow for interpretation of studies of U(VI) bioreduction in the presence of β-$MnO_{2(s)}$. Uranyl bioreduction to $UO_{2(s)}$ by CN32 with H_2 as the electron donor followed Monod kinetics, with a maximum specific reduction rate of 110 μM/h/10^8 cells/mL and a half-saturation constant of 370 μM. The bioreduction rate of β-$MnO_{2(s)}$ by CN32 was described by a pseudo-first-order model with respect to β-$MnO_{2(s)}$ surface sites, with a rate constant of 7.92×10^{-2} h^{-1}/10^8 cells/mL. Uraninite that precipitated as a result of microbial U(VI) reduction was abiotically reoxidized to U(VI) by β-$MnO_{2(s)}$, with concomitant reduction to Mn(II). The oxidation of biogenic $UO_{2(s)}$ coupled with β-$MnO_{2(s)}$ reduction was well-described by an electrochemical model. However, a simple model that coupled the bacterial reduction of U(VI) and β-$MnO_{2(s)}$ with an abiotic redox reaction between $UO_{2(s)}$ and β-$MnO_{2(s)}$ failed to describe the mass loss of U(VI) in the presence of β-$MnO_{2(s)}$. Transmission electron microscopy (TEM) and energy dispersive spectroscopy (EDS) revealed that the particle size and spatial distribution of the biogenic $UO_{2(s)}$ changed dynamically in systems with, as compared to without, β-$MnO_{2(s)}$. These observations suggested that the surface properties and localization of $UO_{2(s)}$ in relation to the cell and β-$MnO_{2(s)}$ surfaces was an important factor controlling the abiotic oxidation of $UO_{2(s)}$ and, thus, the overall rate and extent of U(VI) bioreduction. The coupled model that was modified to account for the "effective" contact surface area between $UO_{2(s)}$ and β-$MnO_{2(s)}$ significantly improved the simulation of microbial reduction of U(VI) in the presence of β-$MnO_{2(s)}$.

Introduction

Dissimilatory metal-reducing bacteria (DMRB) can immobilize uranium by enzymatically reducing U(VI) to insoluble U(IV)$O_{2(s)}$ under anoxic, circumneutral pH conditions (*1*−*3*). DMRB can also use other metals as terminal electron acceptors, including Fe(III) and Mn(III)/Mn(IV) oxides (*4*, *5*) that function as redox buffering phases in soils and aquifer materials. Understanding the influence of these metal oxides on the kinetics and mechanisms of microbial reduction of U(VI) is important for assessing the feasibility of in-situ immobilization of uranium in subsurface environments.

The overall rates of microbial reduction of U(VI) have been observed to decrease in the presence of metal oxides, such as hydrous ferric oxide (HFO) (*6*, *7*), goethite (*8*), Mn(III)/Mn(IV) oxides (*9*), and natural Fe(III)-containing sediments (*7*). Two alternative processes have been proposed to be responsible for this effect: (1) metal oxides compete directly with U(VI) for electrons from actively respiring DMRB (*6*, *9*), and (2) U cycles between the +6 and +4 oxidation states and, thus, functions as electron shuttle between the DMRB and the metal oxides (*7*). The first process decreases the rates of direct enzymatic reduction of U(VI), while the second decreases the overall rates of U(VI) mass loss due to the abiotic reoxidation of U(IV). The importance of the first process was supported by observations that less U(VI) was reduced and more Fe(II) produced with the more bioavailable Fe(III) phase, HFO (*6*), relative to the crystalline Fe(III) oxide, goethite (*6*, *8*). The observation that Fe(III) oxides were more reducible in the U(VI) reduction system (*7*) supported the second process because soluble U(VI) is likely more accessible as an electron acceptor for bacteria than poorly soluble Fe(III) oxides.

Although these two processes have individually been attributed to cause decreases in the rates of microbial reduction of U(VI) in the presence of metal oxides, both may be operative and simultaneously affect U(VI) bioreduction. Quantitative studies, however, have not been performed to determine which process is dominant and whether these processes, when coupled with rate data for microbial reduction of U(VI), can describe the experimental results of U(VI) bioreduction in the presence of metal oxides.

Another process that may affect the overall bioreduction of U(VI) is the abiotic reduction of U(VI) by biogenic Fe(II). Although dissolved Fe(II) is not an efficient reductant of U(VI), U(VI) can be rapidly reduced by Fe(II) coordinated on the Fe(III) oxide surface (*10*). This process, if functioning during the bioreduction of U(VI) and Fe(III) oxide mixtures, could serve to shuttle electrons from DMRB to U(VI) via sorbed or structural Fe(II). However, this process cannot thermodynamically coexist with its reverse process, the reduction of Fe(III) oxides through the electron shuttling by the U(VI)/U(IV) redox pair. Environmental and thermodynamic conditions, reactant and product concentrations, and Fe(II) sorption and localized surface catalysis may all affect redox interactions between U(VI)/U(IV) and Fe(III)/Fe(II) couples.

In this study, we examined the bioreduction of U(VI) by the DMRB, *Shewanella putrefaciens* CN32 in the presence of pyrolusite (β-$MnO_{2(s)}$) in a pH 7.0 bicarbonate buffer. Both U(VI) and β-$MnO_{2(s)}$ are electron acceptors for CN32 (*8*, *9*). Mn(III/IV) oxides are common secondary phases in soils and sediments, and pyrolusite was used as a model Mn(IV) oxide because its stoichiometric, thermodynamic, and structural properties are well-established. Mn(III/IV) oxides are relatively strong oxidants; calculations (*8*, *9*) indicate that U(IV) oxidation by β-$MnO_{2(s)}$ is thermodynamically favorable over a wide range of reactant and product concentrations at neutral pH in bicarbonate-based solutions:

* Corresponding author phone: (509) 376-0129; fax: (509) 376-3650; e-mail: chongxuan.liu@pnl.gov. Address: Pacific Northwest National Laboratory, P.O. Box 999, MSIN K8-96, Richland, WA 99352.

10.1021/es011159u CCC: $22.00 © 2002 American Chemical Society
Published on Web 02/16/2002

This article is a U.S. government work, and is not subject to copyright in the United States.

$$UO_{2(s)} + \beta\text{-}MnO_{2(s)} + H^+ + 3HCO_3^- = Mn^{2+}_{(aq)} + UO_2(CO_3)_3^{4-}{}_{(aq)} + 2H_2O \qquad \log K = 17.79 \quad (1)$$

The objectives of this study were to (1) quantify the kinetics of the individual reactions involved in the microbial reduction of U(VI) in the presence of β-$MnO_{2(s)}$, including the microbial reduction of U(VI) and β-$MnO_{2(s)}$ and the abiotic oxidation of U(IV) by β-$MnO_{2(s)}$; (2) examine the relative importance of β-$MnO_{2(s)}$ as a direct electron acceptor or as an indirect one through U(VI)/U(IV) electron shuttling; and (3) determine whether the overall microbial reduction of U(VI) in the presence of β-$MnO_{2(s)}$ could be described by the coupling of these individual reactions.

Experimental Procedures

Materials. Pyrolusite (β-$MnO_{2(s)}$) was synthesized by a modification of the method by Stahl and James (*11*) and had a surface area of 0.9 $m^2\ g^{-1}$. Uraninite ($UO_{2(s)}$) was generated from the microbial reduction of uranyl acetate in a bicarbonate buffer with *S. putrefaciens* strain CN32 and H_2 as the electron donor. The $UO_{2(s)}$ solids were treated with 10% NaOH to remove cells and organic debris and washed 3 times in 0.1 M Na perchlorate and 2 times in anaerobic deionized H_2O. X-ray diffraction analysis indicated that the resulting solid was uraninite and that the diffraction pattern was identical to that previously reported for biogenic uraninite (*8*).

S. putrefaciens strain CN32 is a DMRB that was isolated from an anaerobic aquifer in northwestern New Mexico. CN32 was routinely cultured aerobically in tryptic soy broth (TSB), 30 g/L (Difco Laboratories, Detroit, MI) and harvested at the mid- to late-exponential growth phase by centrifugation from TSB culture. The harvested cells were washed twice with cold 30 mM PIPES buffer, once with 30 mM bicarbonate buffer, and resuspended in anaerobic bicarbonate buffer (30 mM $NaHCO_3$).

Bacterial Reduction Experiments. Uranium(VI) reduction with and without β-$MnO_{2(s)}$ was studied in 10 mL, 30 mM $NaHCO_3$ batch cultures under conditions of nongrowth with pressurized H_2 as the electron donor. The medium was dispensed into balsch tubes and purged with N_2/CO_2 (80:20) (gases were passed through a column of copper filings to remove trace oxygen to below the detection limit, 50 ppb), stoppered with butyl rubber closures, and crimp-sealed. CN32 cells ($(2-4) \times 10^8$ cells/mL) were exposed to variable uranyl acetate concentrations (50−1200 μM) and incubated anaerobically at 25 °C with 60 rpm rotary shaking. The same medium with variable U(VI) concentrations (0−1100 μM) was used to study the influence of β-$MnO_{2(s)}$ (50 mM or 4.35 g/L, or 3.91 m^2 of surface area/L) on U(VI) reduction. Replicate subsamples of suspension (1 mL) were removed at selected time points in an anaerobic glovebag (Coy Laboratory Products Inc., Grass Lake, MI) with a needle and syringe. The samples were filtered through 0.2 μm polycarbonate filters. The filtrate was analyzed for U(VI) using a kinetic phosphorescence analyzer (*12*) (KPA-10, Chemchek Inst., Richland, WA) and for Mn(II) by inductively coupled plasma (ICP) emission spectroscopy. Total Mn(II) [$Mn(II)_{tot}$] was determined by extraction with 10 mM $CuSO_4$ [$Mn(II)_{(aq)}$ + sorbed Mn(II)] or 0.5 N HCl [Mn(II)(aq) + sorbed Mn(II) + $MnCO_{3(s)}$] (*9*) and analysis by ICP. The two Mn(II) extraction methods yield similar $Mn(II)_{tot}$ values when $MnCO_{3(s)}$ is not present.

Redox Reaction Between β-$MnO_{2(s)}$ and Biogenic $UO_{2(s)}$. The abiotic oxidation of $UO_{2(s)}$ by β-$MnO_{2(s)}$ was investigated under similar conditions to the U(VI) bioreduction experiments, except that the suspension contained 30 mM $NaHCO_3$, 50 mM β-$MnO_{2(s)}$, and variable concentrations of biogenic $UO_{2(s)}$ (100−1200 μM). The production of U(VI), $Mn(II)_{tot}$, and aqueous Mn(II) were monitored at select time points using the same methods described previously.

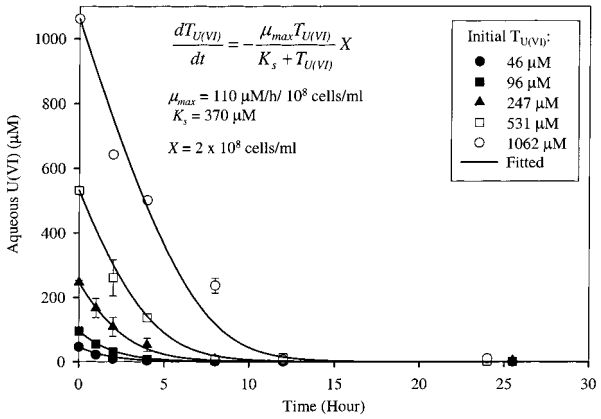

FIGURE 1. Experimental and simulated $U(VI)_{(aq)}$ concentrations as a function of time and initial $U(VI)_{(aq)}$ concentrations in batch cultures of *S. putrefaciens* strain CN32 (H_2 as electron donor).

Sorption Measurements. The sorption of Mn(II) by pyrolusite was measured under anaerobic conditions in glass pressure tubes as a function of Mn(II) concentration (0−1 mM) on 50 mM β-$MnO_{2(s)}$ (4.35 g, or 3.91 m^2 of surface area). PIPES (1,4-piperazinediethanesulfonic acid) buffer was used instead of bicarbonate buffer to avoid rhodocrosite precipitation. All samples were allowed to equilibrate for 1 h under continuous mixing (100 rpm). After equilibration, the suspensions were filtered (0.2 μm) and the filtrate acidified (1 N HCl). Mn(II) in the acidified filtrates was measured by ICP. Sorbed Mn(II) was calculated from the difference between the total and final aqueous Mn(II) concentrations.

Transmission Electron Microscopy. Samples for high-resolution transmission electron microscopy (TEM) were prepared in an anaerobic glovebox to avoid oxidation of U(IV) and Mn(II). Cell suspensions were washed 3 times with 0.1 M sodium cacodylate buffer at pH 7.2 followed by 3 washes with cold deionized water. The cells were gently pelleted, fixed in glutaraldehyde, dehydrated by washing in ethanol, and embedded in LR White resin. The polymerized blocks were anaerobically sectioned on a microtome, and thin sections were mounted on copper grids coated with Formvar and carbon. The traditional osmium tetraoxide postfixation step, as well as poststaining with uranyl acetate/lead citrate, was completely omitted. To compensate for the dramatic decrease in the contrast of a biological sample portion, we used the smallest possible apertures on a JEOL 2010 TEM. Samples were sealed in airtight container and exposed to aerobic conditions for less than 1 min while being transferred to the high-vacuum sample chamber of the JEOL 2010 TEM. The preparations were examined with an acceleration voltage of 200 kV. The elemental composition of cell-associated precipitates was determined using energy dispersive spectroscopy (EDS) (Oxford Instruments).

Results and Discussion

U(VI) Bioreduction. Uranyl reduction by CN32 was effectively described by Monod kinetics with no growth (Figure 1 and eq 2),

$$\frac{dT_{U(VI)}}{dt} = -\frac{\mu_{max} T_{U(VI)}}{K_s + T_{U(VI)}} X \qquad (2)$$

where $T_{U(VI)}$ is the total U(VI) concentration (μM), μ_{max} is the maximum specific reduction rate (μM/h/cells/mL), K_s is the half-saturation constant (μM), and X is the cell concentration (cells/mL). A lag phase, which was reported with a sulfate reducing bacteria, *Desulfovibrio desulfuricans* (ATCC7757)

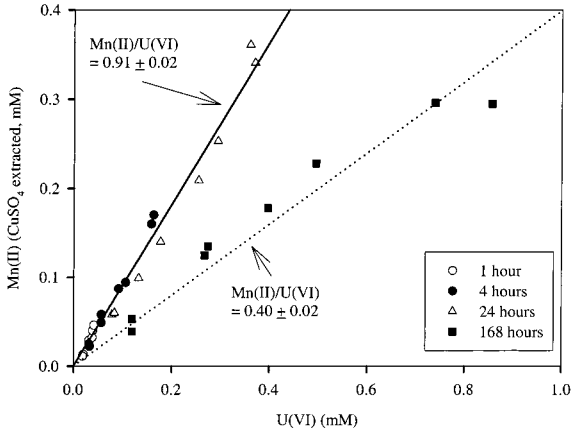

FIGURE 2. Ratio of Mn(II) and U(VI) concentrations produced from abiotic oxidation of biogenic $UO_{2(s)}$ by β-$MnO_{2(s)}$. The plot shows the ratio of Mn(II)/U(VI) as a function of sampling time.

(*13*), was not observed here. The U(VI) reduction began immediately after inoculation (Figure 1) and continued until the U(VI) was completely reduced. The maximum specific reduction rate (μ_{max}) and half-saturation constant (K_s) were estimated to be 110 μM/h/10^8 cells/mL and 370 μM, respectively, by nonlinear fitting of eq 2 to the experimental data with variable initial U(VI) concentrations (Figure 1). Using a dry cell weight of 6.4×10^{-10} mg/cell, the estimated maximum specific reduction rate was equivalent to 1.72 mM/h/mg/mL cells, which was close to the reported value of 1.38 mM/h/mg/mL for *Desulfovibrio desulfuricans* (*13*). The half-saturation constants were also comparable, 0.37 mM (Figure 1) versus 0.25 mM (*13*).

Abiotic Oxidation of Biogenic Uraninite by β-$MnO_{2(s)}$. *Mn(II)/U(VI) Ratio*. Biogenic $UO_{2(s)}$ was oxidized by β-$MnO_{2(s)}$. The ratio of the redox reaction end products, Mn(II) and U(VI), averaged 0.91 ± 0.02 within 24 h of the reaction initiation (Figure 2). This ratio decreased to 0.40 ± 0.02 at 168 h, possibly due to the precipitation of rhodochrosite ($MnCO_{3(s)}$) and the inability of the $CuSO_4$ extraction to access this Mn(II). Speciation calculations using MINTEQA2 with a U(VI) species database compiled by the authors indicated that rhodochrosite was the only supersaturated mineral phase when $Mn(II)_{(aq)}$ exceeded 50 μM. The Mn(II)/U(VI) ratio of 0.91 is stoichiometrically correspondent to the reduction of β-$MnO_{2(s)}$ and oxidation of $UO_{2.09(s)}$. Previous studies indicated that the biogenic uraninite contains some U(VI) and has an apparent molecular form of $UO_{2+x(s)}$, where x can range from 0 to 0.17 (*6*).

Sorption of Mn(II). The sorption of Mn(II) on pyrolusite determined during the course of the abiotic oxidation of $UO_{2+x(s)}$ by β-$MnO_{2(s)}$ yielded a linear isotherm with an apparent distribution coefficient (K_d) of 3.4 (±0.2) × 10^{-3} mM/mM of β-$MnO_{2(s)}$ or 0.039 ± 0.002 L/g (Figure 3a). The concentration of $UO_{2+x(s)}$ had little or no effect on Mn(II) sorption by β-$MnO_{2(s)}$ (Figure 3a). The same approximate K_d value was also observed after 168 h of reduction (Figure 3a), suggesting that the effects of rhodochrosite precipitation and U(VI) production had negligible effects on Mn(II) sorption. The linear adsorption behavior of Mn(II) resulted from its relatively low concentration (<0.35 mM equilibrium aqueous concentration) in relation to the surface site concentration of β-$MnO_{2(s)}$. Surface sites became saturated when $Mn(II)_{(aq)}$ was >1 mM (Figure 3b). A surface density of 13 complexation sites/nm^2 was calculated from the fitted maximum sorption capacity of Mn(II) on β-$MnO_{2(s)}$ (Figure 3b) and its surface area (0.9 m^2/g). This surface density was somewhat greater than reported for most oxides (4−10 sites/nm^2) (*14*) but close to the reported number, 15−20 Mn(II) sites/nm^2, for birnessite (δ-$MnO_{2(s)}$) (*15*). The Langmuir isotherm determined

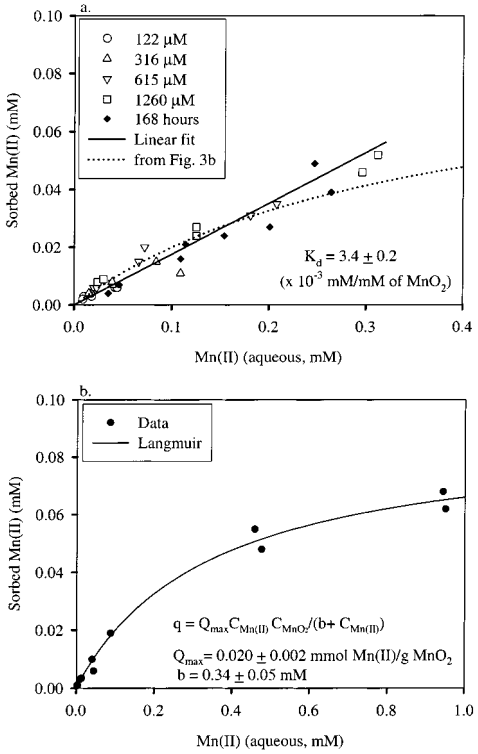

FIGURE 3. (a) Mn(II) sorption observed during the abiotic oxidation of $UO_{2(s)}$ by β-$MnO_{2(s)}$ with variable $UO_{2(s)}$ concentrations. (b) Sorption of Mn(II) on β-$MnO_{2(s)}$ and a Langmuir isotherm fit of the data.

from Figure 3b closely matched the experimental results of Mn(II) sorption on β-$MnO_{2(s)}$ during uraninite oxidation (Figure 3a).

Initial Rate of Abiotic $UO_{2(s)}$ Oxidation by β-$MnO_{2(s)}$. The abiotic oxidation of $UO_{2(s)}$ in spent nuclear fuel has been extensively studied. The kinetics of $UO_{2(s)}$ oxidation have been described with an electrochemical (or corrosion) model (*16*−*23*). The reaction scheme in this model with bicarbonate buffer can be described with two primary steps (A and B) where ">" denotes a surface complex.

(A) $UO_{2(s)}$ oxidation:

$$>U(IV)O_{2(s)} + CO_3^{2-}{}_{(aq)} = >U(VI)O_2CO_{3(s)} + 2e^- \quad (3)$$

(B) U(VI) detachment:

$$>U(VI)O_2CO_{3(s)} + 2CO_3^{2-}{}_{(aq)} = U(VI)O_2(CO_3)_3^{4-}{}_{(aq)} \quad (4)$$

The electron-transfer reaction 3 is a rate-limiting step in bicarbonate buffer (*16*, *21*, *23*−*25*). Various models based on different mechanistic schemes for reaction 3 have been proposed. We used the relatively simple model of Nicol and Needes (*16*) that is based on the measurement of the anodic current and the $UO_{2(s)}$ oxidation product with the assumption that reaction 3 could be treated as an elemental reaction. Under this reaction scheme, and after coupling with the associated reduction reaction of β-$MnO_{2(s)}$ (*15*) (expressed as oxidation reaction),

$$Mn^{2+}{}_{(aq)} + 2H_2O = \beta - MnO_{2(s)} + 2e^- + 4H^+ \quad (5)$$

an electrochemical model was obtained for the U(VI)/U(IV) − Mn(IV)/Mn(II) system

$$dU(VI)/dt = i_{UO_2}A_{UO_2}/2F = -i_{MnO_2}A_{MnO_2}/2F \quad (6)$$

where i_{UO_2} and i_{MnO_2} are the current density (mA/m^2) on the

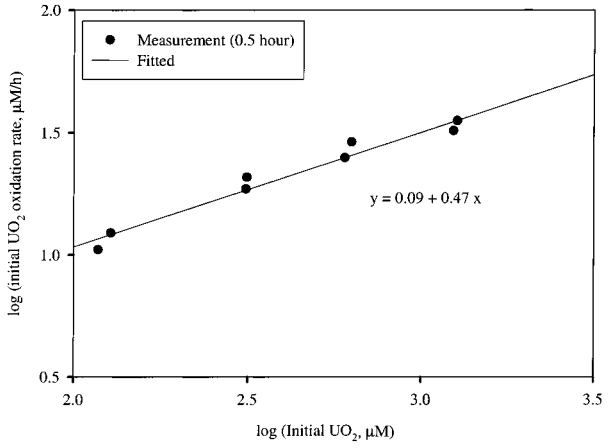

FIGURE 4. Initial rates of $UO_{2(s)}$ oxidation by β-$MnO_{2(s)}$ as a function of initial $UO_{2(s)}$ concentrations.

$UO_{2(s)}$ and β-$MnO_{2(s)}$ surfaces, A_{UO_2} and A_{MnO_2} are surface areas (m^2/L), and F is the faraday constant. The current density (i) can be described by the Bulter−Volmer expression with the simplification of electron-transfer coefficients (*21*)

$$i_{UO_2} = 2Fk_1\{CO_3^{2-}\}\exp(E_mF/2RT) - 2Fk_{-1}\exp(-E_mF/2RT) \quad (7)$$

$$i_{MnO_2} = 2Fk_2\{Mn^{2+}\}\exp(E_mF/2RT) - 2Fk_{-2}\{H^+\}^4\exp(-E_mF/2RT) \quad (8)$$

where E_m is the excess (relative to equilibrium) electron potential across the $UO_{2(s)}$ and β-$MnO_{2(s)}$ interfaces; R is the gas constant; T is the temperature; k_1 and k_{-1} and k_2 and k_{-2} are forward and backward rate coefficients for reactions 3 and 5, respectively; and { } denotes activity. Algebraic manipulation of eq 6 through eq 8 yields

$$\frac{dC_{U(VI)}}{dt} = A_{UO_2}A_{MnO_2}[k_{-2}k_1\{CO_3^{2-}\}\{H^+\}^4 - k_2k_{-1}\{Mn^{2+}\}]/[[A_{MnO_2}k_{-2}\{H^+\}^4 + A_{UO_2}k_{-1}]^{1/2}[A_{MnO_2}k_2\{Mn^{2+}\} + A_{UO_2}k_1\{CO_3^{2-}\}]^{1/2}] \quad (9)$$

The initial oxidation rate was obtained after neglecting the reverse electron transfer [from Mn(II) to U(VI)] of reactions 3 and 5

$$\frac{dC_{U(VI)}}{dt} = (A_{UO_2}A_{MnO_2}k_1k_{-2}\{CO_3^{2-}\}\{H^+\}^4)^{0.5} \quad (10)$$

Equation 10 indicated that the reaction order with respect to bicarbonate concentration and surface area of $UO_{2(s)}$ was the square root. A value of 0.46 has been observed in the extensive studies on $UO_{2(s)}$ oxidation in the carbonate system when the electron-transfer step is limiting the overall $UO_{2(s)}$ oxidation rate (*21*). Other experimental results indicate that this value is in the range of 0.4−0.7 (*20*, *25*).

The reaction order of the initial biogenic uraninite oxidation coupled with β-$MnO_{2(s)}$ reduction was 0.47 ± 0.04 with respect to $UO_{2(s)}$ concentration (Figure 4) when β-$MnO_{2(s)}$ was fixed at 50 mM. The initial rates in Figure 4 were calculated using measured U(VI) concentration changes from time 0 to 0.5 h. Assuming that the specific surface area of $UO_{2(s)}$ did not change significantly during the initial stages of oxidation, then the reaction order of our results was close to that predicted by eq 10.

Equation 9 was derived under the assumption that the electron-transfer step in $UO_{2(s)}$ oxidation proceeds as in reaction 3. A variety of two-step reaction schemes have been proposed for oxidative electron transfer, including (1) U(IV)$O_{2(s)}$ oxidation to U(V)$O_2HCO_{3(s)}$ and then to $UO_2CO_{3(s)}$ (*21*); (2) U(IV)$O_{2(s)}$ oxidation to $UO_{2.33(s)}$, a mixture of U(VI) and U(IV), with subsequent reaction to $UO_2CO_{3(s)}$ (*17*, *20*, *23*); and (3) direct oxidation of U(IV)$O_{2(s)}$ to U(VI)$O_{3(s)}$, followed by surface complex formation with carbonate (*25*). Algebraic manipulation demonstrated that the initial rates of $UO_{2(s)}$ oxidation from the first two, two-step reaction schemes had similar rate dependencies to eq 10 after coupling with oxidant reduction (i.e., about half-order with respect to $UO_{2(s)}$ surface area and carbonate concentration). The initial rate based on the third reaction scheme, however, was different and showed first-order dependence on U(IV)$O_{2(s)}$ surface area. Because of the multiple electron-transfer steps involved in the first two reaction schemes, the development of an exact electrochemical model is complicated (*21*), and such models often have to be simplified in order to describe experimental results (*22*, *26*). In this study, eq 9 was used as our first choice in modeling the abiotic redox reaction of U(IV) and β-$MnO_{2(s)}$ because of its relative simplicity and its ability to describe the initial rate of $UO_{2(s)}$ oxidation. As shown later (next section), this model also well described $UO_{2(s)}$ oxidation coupled with β-$MnO_{2(s)}$ reduction.

Parameter Determination. Model 9 contains 4 parameters. However, only two of these are independent because the forward and backward rate constants are related by thermodynamic equilibrium constants. By redefining the rate parameters in eq 9 as

$$k'_1 = k_1S_{UO_2}, \quad k'_{-1} = k_{-1}S_{UO_2}, \quad k'_2 = k_2S_{MnO_2}, \quad k'_{-2} = k_{-2}S_{MnO_2}$$

where S_{UO_2} and $S_{\beta-MnO_2}$ are specific surface areas (m^2/μmol) for uraninite and pyrolusite, respectively, then eq 9 becomes

$$\frac{dC_{U(VI)}}{dt} = C_{UO_2}C_{\beta-MnO_2}[k'_{-2}k'_1\{CO_3^{2-}\}\{H^+\}^4 - k'_2k'_{-1}\{Mn^{2+}\}]/[[C_{\beta-MnO_2}k'_{-2}\{H^+\}^4 + C_{UO_2}k'_{-1}]^{1/2}[C_{\beta-MnO_2}k'_2\{Mn^{2+}\} + C_{UO_2}k'_1\{CO_3^-\}]^{1/2}] \quad (11)$$

where C_{UO_2} and $C_{\beta-MnO_2}$ are the concentrations of $UO_{2(s)}$ and β-$MnO_{2(s)}$ (μM), respectively. The kinetic constants of k'_1 and k'_{-1} are related by reaction 3 at equilibrium,

$$k'_1/k'_{-1} = \exp(-\Delta G_0^r/RT) = 10^{0.59}\ (M^{-1}) = 10^{-5.41}\ (\mu M^{-1}) \quad (12)$$

and k'_2 and k'_{-2} are related by eq 5,

$$k'_{-2}/k'_2 = \exp(\Delta G_0^r/RT) = 10^{41.56}\ (M^{-3}) = 10^{23.56}\ (\mu M^{-3}) \quad (13)$$

where ΔG_0^r is free energy for reactions 3 or 5. The results in Figure 4 provide another constraint based on eq 10,

$$C_{\beta-MnO_2}k'_1/k'_{-2}\{H^+\}^4\{CO_3^{2-}\} = 1.23\ \mu M\ h^{-2} \quad (14)$$

Therefore, only one parameter in eq 11 has to be determined from experimental data.

Model 11 well described the experimental abiotic oxidation of biogenic $UO_{2(s)}$ (Figure 5a) and β-$MnO_{2(s)}$ reduction (parts b and c of Figure 5). The best-fitted parameter of k'_1 was $2.70 \times 10^{-12}\ h^{-1}\ \mu M^{-1}$. From eq 12−14, we calculated $k'_{-1} = 6.94 \times 10^{-7}\ h^{-1}$, $k'_2 = 1.79 \times 10^{-14}\ h^{-1}\ \mu M^{-1}$, and $k'_{-2} = 6.49 \times 10^9\ h^{-1}\ \mu M^{-4}$.

***β*-MnO$_{2(s)}$ Bioreduction by CN32**. The sorption of Mn(II) during β-MnO_2 bioreduction, determined from the difference

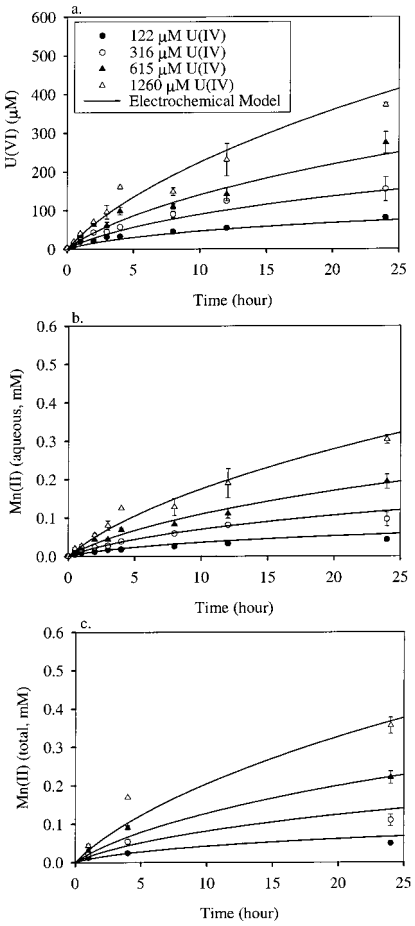

FIGURE 5. Experimental data and model simulation of $U(VI)_{(aq)}$ and Mn(II) production from the abiotic oxidation of $UO_{2(s)}$ by β-$MnO_{2(s)}$ (50 mM) with variable initial $UO_{2(s)}$ concentrations: (a) $U(VI)_{(aq)}$ production, (b) aqueous Mn(II), and (c) aqueous and sorbed Mn(II).

between the extracted and the aqueous Mn(II), displayed a linear trend (aqueous Mn(II) < 0.035 mM) with a ratio of $Mn(II)_{sb}(mM)/Mn(II)_{aq}(mM) = 2.48$ (Figure 6a). It was assumed that the total sorbed Mn(II) concentration was an additive function of Mn(II) sorption on β-$MnO_{2(s)}$ and CN32

$$Mn(II)_{sb}/Mn(II)_{aq} = (Mn(II)_{sb}(\beta\text{-}MnO_{2(s)}) + Mn(II)_{sb}(CN32))/Mn(II)_{aq}$$

The ratio $Mn(II)_{sb}(\beta\text{-}MnO_{2(s)})/Mn(II)_{aq}$ was estimated to be 0.17 using the K_d value 3.4×10^{-3} mM/mM of β-$MnO_{2(s)}$ determined in Figure 3a. This value, in turn, allowed us to calculate that the $Mn(II)_{sb}(CN32)/Mn(II)_{aq}$ ratio in the bioreduction experiment was 2.31. Using the ratio of 2.31, the calculated concentration of Mn(II) sorbed on CN32 was 0.1 mmol/L at 45 μmol/L of $Mn(II)_{aq}$. This value was less than the available surface sites on CN32 (0.84 mM) estimated for a cell concentration of 2×10^8 cells/mL from the reported site density of CN32 (*27*). The affinity coefficient for the surface complexation reaction

$$Mn(II) + {>}cell = {>}cell{-}Mn(II) \qquad \log K$$

was estimated to be $\log K = 3.44$. This value was similar to that measured for Fe^{2+} on CN32 under comparable conditions ($\log K$ (>cell−Fe(II)) = 3.29) (*27*).

The $Mn(II)_{aq}$ concentration resulting from the reduction of β-$MnO_{2(s)}$ by CN32 increased linearly with time (Figure 6b). This pseudo-zero-order rate was consistent with the previous observation of goethite reduction by CN32 (*28*).

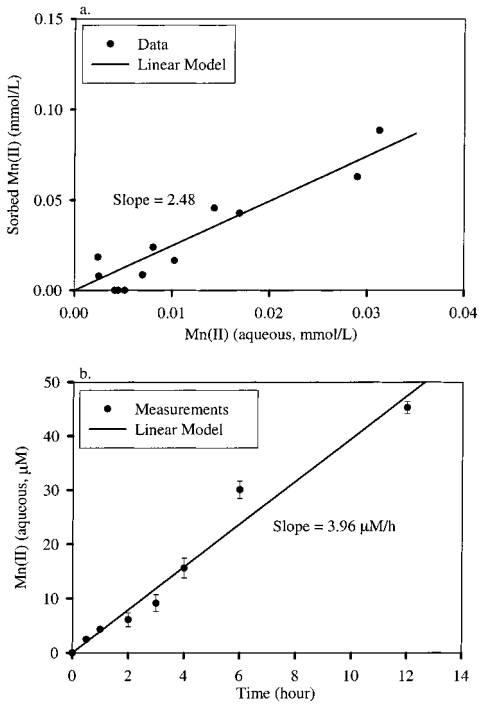

FIGURE 6. (a) Sorption of Mn(II) in the suspension of CN32, $U(VI)_{(aq)}$, and β-$MnO_{2(s)}$. (b) $Mn(II)_{(aq)}$ production from reduction of β-$MnO_{2(s)}$ as a function of time in a pure culture of CN32 (β-$MnO_{2(s)}$ = 50 mM, H_2 as electron donor).

According to (*28*), the rate of microbial reduction of goethite followed a pseudo-first-order rate with respect to surface site concentration. For the Mn(IV) oxide studied here, the rate expression can be approximated as

$$\frac{dC_{MnO_2}}{dt} = -k_1[{>}\beta\text{-}MnO_{2(s)}][cell] \qquad (15)$$

Because the aqueous Mn(II) concentration was small (<50 μM) relative to the estimated surface site concentration of β-$MnO_{2(s)}$ (Figure 6b), the degree of surface saturation was estimated to be less than 10% on the basis of the estimated sorption maximum (Figure 3). Therefore, after approximating [>β-$MnO_{2(s)}$] with the total site concentration of β-$MnO_{2(s)}$ in eq 15, the reduction rate became pseudo-zero-order under our specific experimental conditions (e.g., no growth). The fitted zero-order rate coefficient, $k_0 = k_1$ [>β-$MnO_{2(s)}$], was 6.89 μM/h/10^8 cells/mL. By approximating [>β-$MnO_{2(s)}$] with maximum Mn(II) sorption site concentration (Figure 3b), the pseudo-first-order rate coefficient was estimated to be 0.079 $h^{-1}/10^8$ cells/mL. This reduction rate was larger than the microbial reduction rate of goethite by CN32 (0.029 $h^{-1}/10^8$ cells/mL) (*28*) but was about 15-fold slower than the maximum U(VI) reduction rate by CN32 (Figure 1). The faster reduction rate observed here for β-$MnO_{2(s)}$ as compared to goethite (*28*) may relate to our usage of H_2 as an electron donor in this study, while lactate was used in the former one. Hydrogen supports faster reduction rates of Tc (*29*−*31*) and other metals [Fe(III), Co(III), U(VI) (*31*)] than does lactate. The slower microbial reduction of β-$MnO_{2(s)}$ as compared to U(VI) was consistent with the concept that aqueous-phase electron acceptors are more accessible for microbial reduction than solid-phase ones.

Simulation of U(VI) Reduction by CN32 in the Presence of β-$MnO_{2(s)}$. The microbial reduction of U(VI) was impeded by the presence of β-$MnO_{2(s)}$ (Figure 7), and the presence of U(VI), in turn, facilitated the generation of Mn(II) (Figure 8). The apparent decrease in U(VI) concentration was much

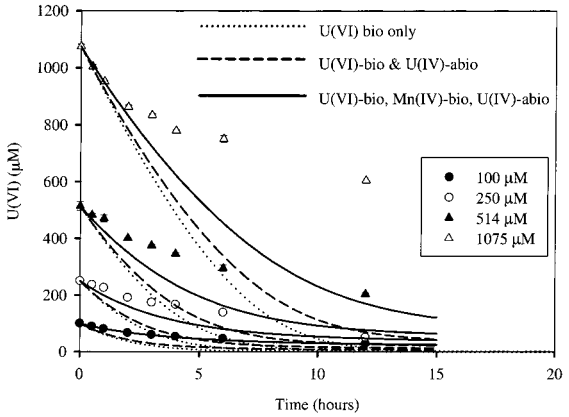

FIGURE 7. Experimental data and model-predicted U(VI) concentrations as a function of time and initial $U(VI)_{(aq)}$ concentration in the mixed suspension of $U(VI)_{(aq)}$, β-$MnO_{2(s)}$ (50 mM), and CN32 (H_2 as electron donor).

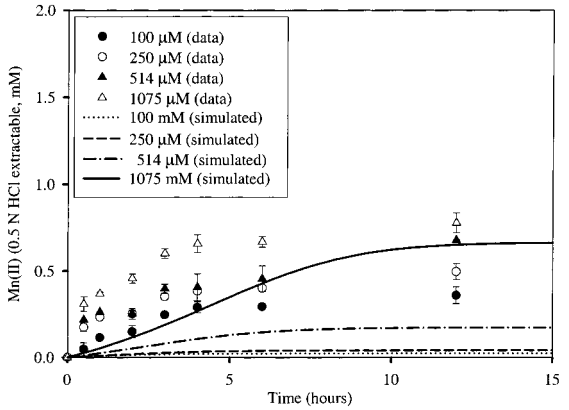

FIGURE 8. Experimental and model-predicted maximum Mn(II) concentration as a function of time and initial $U(VI)_{(aq)}$ concentration in the mixed suspension of $U(VI)_{(aq)}$, β-$MnO_{2(s)}$ (50 mM), and CN32.

slower than predicted by the Monod rate for bioreduction of U(VI) (eq 2) (dotted lines in Figure 7) or by the coupling of the Monod rate (eq 2) and abiotic redox reaction between β-$MnO_{2(s)}$ and $UO_{2(s)}$ (eq 11) (dashed lines in Figure 7). While the model simulation that coupled the microbial reduction of U(VI) (eq 2) and β-$MnO_{2(s)}$ (eq 15) and the abiotic redox reaction (eq 11) more closely predicted the low initial U(VI) concentration (100 μM), it still poorly predicted the extent of U(VI) reduction at the higher initial U(VI) concentrations (solid lines in Figure 7).

In the latter simulation, the total concentration of microorganisms was partitioned into two population subsets: one that reduced U(VI) and another that reduced β-$MnO_{2(s)}$. The fraction (F) of the total organisms associated with each of these population subsets was calculated from the electron acceptor mole fraction (e.g., $F_{U(VI)} = T_{U(VI)}/(T_{U(VI)} + [>\beta\text{-}MnO_{2(s)}])$ and $F_{MnO_2} = [>\beta\text{-}MnO_{2(s)}]/(T_{U(VI)} + [>\beta\text{-}MnO_{2(s)}])$. On the basis of the total number of surface sites ($>\beta$-$MnO_{2(s)}]_T$), estimated for β-$MnO_{2(s)}$ from the sorption capacity (13 sites/nm^2), the calculated $F_{U(VI)}$ was 0.24−0.54, 0.38−0.75, 0.70−0.86, and 0.88−0.93 in 100, 250, 514, and 1075 mmol/L of U(VI) treatments, respectively. The coupled model also performed poorly in simulating the evolution of $Mn(II)_{tot}$ using this assumption (Figure 8). In general, the $Mn(II)_{tot}$ was significantly underpredicted by the model.

The discrepancy between the predicted and observed values could not be improved by simply adjusting the fraction of active cells associated with reducing U(VI) or β-$MnO_{2(s)}$ (e.g., $F_{U(VI)}$ or F_{MnO_2}). Increasing F_{MnO_2} decreased the U(VI) reduction rate and, thus, improved the U(VI) simulation but lead to greater underprediction and, thus, larger disparity in the simulation of the Mn(II) due to the slower rate of direct reduction of β-$MnO_{2(s)}$.

A possible explanation for the difference between the model and the experiment was that the availability of U(IV) for the oxidation by β-$MnO_{2(s)}$ changed with time. TEM images of unstained thin sections of CN32 cell suspensions incubated with U(VI) in the absence of β-$MnO_{2(s)}$ revealed the presence of fine-grained $UO_{2(s)}$ aggregates. These aggregates occurred extracellularly and in association with cell surfaces (Figure 9a) and included a significant mass of $UO_{2(s)}$ that was precipitated within the cell periplasm (Figure 9b). The morphology of the biogenic $UO_{2(s)}$ was significantly different when the cells were incubated with U(VI) in the presence of β-$MnO_{2(s)}$ (parts c and d of Figure 9). Extracellular $UO_{2(s)}$ was absent and curious nodules of $UO_{2(s)}$ were observed in association with the cell surface when the mineral oxidant was present.

On the basis of the TEM observations, the distribution and surface properties of the biogenic $UO_{2(s)}$ may change or evolve during U(VI) reduction in the presence of β-$MnO_{2(s)}$. These changes may be functions of mass transfer, crystallization, localization and aggregation of U(IV), and organism/β-$MnO_{2(s)}$ contact. These factors are not well-understood or easily quantified. It is unclear whether U(IV) is oxidized by β-$MnO_{2(s)}$ in the form of individual ions, disordered precipitate clusters, crystallites, or crystallite aggregates. Including all these factors, if indeed they were quantifiable, would complicate the model and result in large uncertainties regarding the processes and fitted parameters.

As a compromise to acknowledge the changing properties of the biogenic $UO_{2(s)}$, we introduced a factor to account for the "effective" surface area of uraninite that was available for the oxidation by β-$MnO_{2(s)}$. To enact this concept, we introduced a factor β into eq 11, yielding eq 16

$$\frac{dC_{U(VI)}}{dt} = [\beta C_{UO_2} C_{\beta-MnO_2}(k'_{-2}/k'_1\{CO_3^{2-}\}\{H^+\}^4 - k'_2k'_{-1}\{Mn^{2+}\})]/[[C_{\beta-MnO_2}k'_{-2}\{H^+\}^4 + \beta C_{UO_2}k'_{-1}]^{1/2}[C_{\beta-MnO_2}k'_2\{Mn^{2+}\} + \beta C_{UO_2}k'_1\{CO_3^-\}]^{1/2}] \quad (16)$$

The β in eq 16 was treated as the only adjustable parameter in fitting the modified coupled model to the experimental results in Figure 7. As shown in Figure 10, the simulation by the modified model showed far better agreement with the experimental data. The best fitted β value was 40 for the model of U(VI) bioreduction coupling abiotic U(IV) oxidation by β-$MnO_{2(s)}$ and 20 for the coupling of U(VI) and β-$MnO_{2(s)}$ bioreduction with abiotic U(IV) oxidation by β-$MnO_{2(s)}$. These results implied that the effective or reactive surface area of the $UO_{2(s)}$ that was bioprecipitated in the presence of β-$MnO_{2(s)}$ was about 20−40 times greater than that of the biogenic $UO_{2(s)}$ used in the abiotic oxidation experiments (Figure 5). Figure 9 clearly showed that the biogenic $UO_{2(s)}$ produced in absence and presence of β-$MnO_{2(s)}$ was different in morphology and distribution relative to the cell surface. The images, however, did not necessarily justify the high surface area needed to model the U(VI)/β-$MnO_{2(s)}$/CN32 system, unless the Figure 9a material was aggregated when used in the experiment of Figure 5 or unless the surface $UO_{2(s)}$ nodules noted in parts c and d of Figure 9 were fibrous. Our current data does not allow for a resolution of this issue.

Implications to the Kinetics of U(VI) Reduction in the Presence of Metal Oxides. This study demonstrated that the overall rate of U(VI) reduction in DMRB suspensions was decreased by the presence of the Mn(IV) oxide, pyrolusite. Two phenomena, including competition between Mn(IV) and U(VI) as electron acceptors for respiration and U(IV)

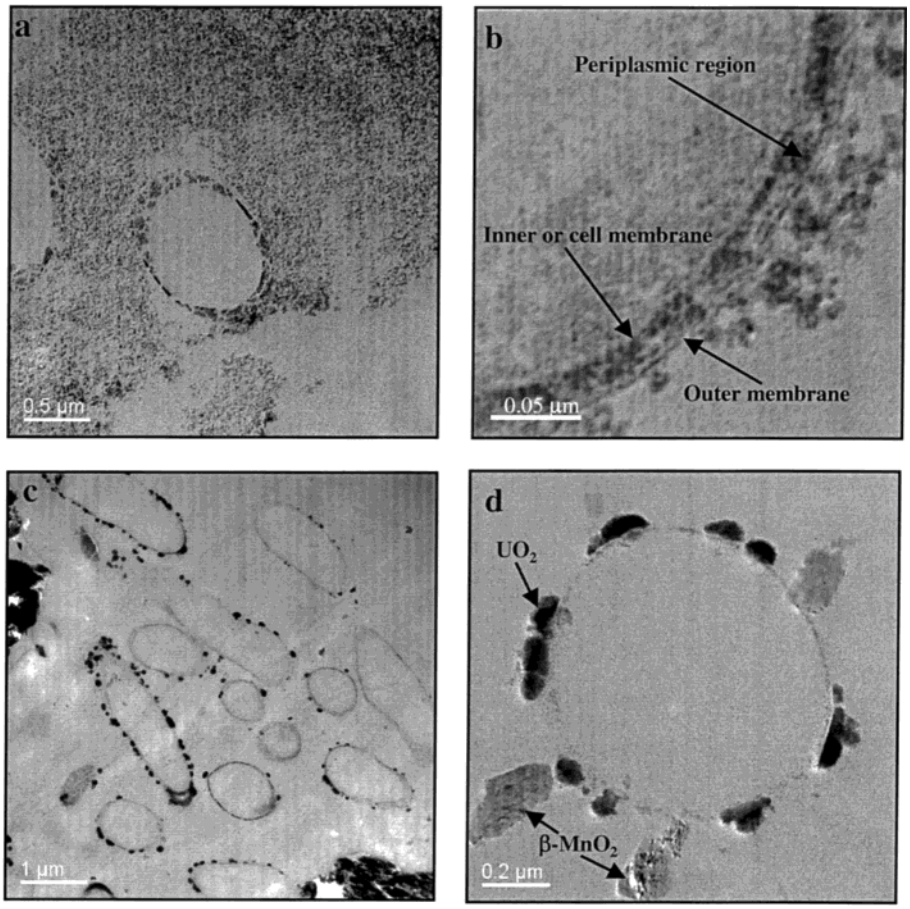

FIGURE 9. TEM images of thin sections of CN32 cells incubated with H_2 and $U(VI)_{(aq)}$ in bicarbonate buffer in the absence of pyrolusite, illustrating the extracellular accumulation of $UO_{2(s)}$ and $UO_{2(s)}$ precipitates at the cell surface and within the periplasmic space in (a) unstained and (b) stained cells. CN32 incubated with H_2 and $U(VI)_{(aq)}$ in the presence of pyrolusite [β-$MnO_{2(s)}$], showing (c) a lack of fine-grained extracellular $UO_{2(s)}$ and (d) accumulation of $UO_{2(s)}$ nodules on the cell surface.

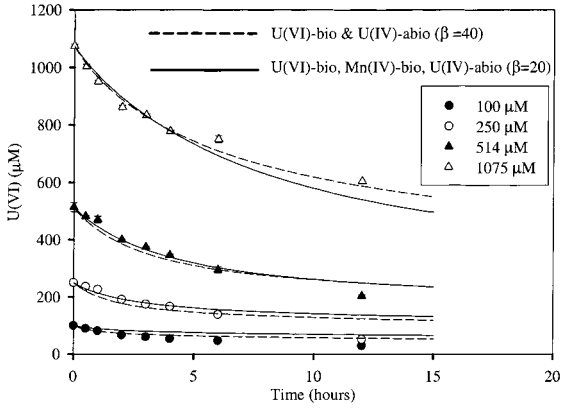

FIGURE 10. Model simulation of $U(VI)_{(aq)}$ concentrations after including an factor (β) to account for the "effective" surface area between biogenic $UO_{2(s)}$ and β-$MnO_{2(s)}$. Other conditions are the same as those in Figure 7.

oxidation by Mn(IV) (electron shuttling), appeared to inhibit U(VI) bioreduction. The shuttling effect of U(VI) appeared to dominate because pyrolusite was poorly bioavailable and $UO_{2(s)}$ was oxidized rapidly when contacted with β-$MnO_{2(s)}$. Competition may be more important for more bioavailable Mn(IV) oxides such as birnessite, that are more commonly found in soils and subsurface sediments. The modeling demonstrated that the overall rate of U(VI) reduction in the presence of β-$MnO_{2(s)}$ was more complicated than the simple linear combination of the individual biotic and abiotic reactions. The complete kinetic description of U(VI) reduction in the presence of polyvalent metal oxides may have to consider additional physical processes and factors not considered in our model such as U(IV) mass transfer, precipitate localization, morphology, crystallization degree, and aggregation.

This investigation and that of Nevin and Lovley (*7*) indicate that the reduction rates of some metal oxides significantly increases in the presence of U(VI). The observed rate of β-$MnO_{2(s)}$ reduction increased with increasing U(VI) concentration (Figure 8) and was 5-fold higher than the direct enzymatic reduction of β-$MnO_{2(s)}$ (eq 15). These observations indicate that the U(VI)/U(IV) redox pair may facilitate metal oxide reduction by DMRB through electron shuttling. This effect, however, is more pronounced for Mn(IV) oxides than the Fe(III) oxides because of the higher E° of the pyrolusite redox couple. For oxides that exhibit greater bioavailability, such as poorly crystalline Fe(III) oxide, direct microbial reduction of the oxide may compete strongly with U(VI) for electrons (*6*). The U(VI)/U(IV) shuttling process is energetically less favorable for Fe(III) oxides and would become thermodynamically unfeasible as biogenic Fe(II) increases. In fact, as Fe(II) accumulates at the Fe(III) oxide surface, sorbed Fe(II) becomes an effective reductant for U(VI) (*8*, *10*).

Acknowledgments

This research was supported by the Natural and Accelerated Bioremediation Research Program (NABIR), Office of Biological and Environmental Research (OBER), and U.S. Department of Energy (DOE). Pacific Northwest National

Laboratory is operated for the DOE by the Battelle Memorial Institute under Contract DE AC06-76 RLO 1830. We thank three reviewers for their valuable comments and suggestions.

Literature Cited

(1) Lovley, D. R.; Phillips, E. J.; Gorby, Y. A.; Landa, E. *Nature* **1991**, *350*, 413−416.
(2) Gorby, Y. A.; Lovley, D. R. *Environ. Sci. Technol.* **1992**, *26*, 205−207.
(3) Lovley, D. R. *Annu. Rev. Microbiol.* **1993**, *47*, 263−290.
(4) Lovley, D. R. *Microbiol. Rev.* **1991**, *55*, 259−287.
(5) Nealson, K.; Saffarini, D. *Annu. Rev. Microbiol.* **1994**, *48*, 311−343.
(6) Wielinga, B.; Bostick, B.; Hansel, C. M.; Rosenzweig, R. F.; Fendorf, S. *Environ. Sci. Technol.* **2000**, *34*, 2190−2195.
(7) Nevin, K. P.; Lovley, D. R. *Environ. Sci. Technol.* **2000**, *34*, 2472−2478.
(8) Fredrickson, J. K.; Zachara, J. M.; Kennedy, D. W.; Duff, M. C.; Gorby, Y. A.; Li, S.-M.; Krupka, K. M. *Geochim. Cosmochim. Acta* **2000**, *64*, 3085−3098.
(9) Fredrickson, J. K.; Zachara, J. M.; Kennedy, D. W.; Liu, C.; Duff, M. C.; Hunter, D. B.; Dohnalkova, A. *Geochim. Cosmochim. Acta* **2002**, in press.
(10) Liger, E.; Charlet, L.; van Cappellen, P. *Geochim. Cosmochim. Acta* **1999**, *63*, 2939−2955.
(11) Stahl, R. S.; James, B. R. *Soil Sci. Soc. Am. J.* **1991**, *55*, 1291−1294.
(12) Brina, R.; Miller, A. G. *Anal. Chem.* **1992**, *64*, 1413−1418.
(13) Spear, J. R.; Figueroa, L. A.; Honeyman, B. D. *Environ. Sci. Technol.* **1999**, *33*, 2667−2675.
(14) Sigg, L.; Stumm, W. *Colloids Surf.* **1980**, *2*, 101−117.
(15) Stone, A. T.; Ulrich, H.-J. *J. Colloid Interface Sci.* **1989**, *132*, 509−522.
(16) Nicol, M. J.; Needes, C. R. S. *Electrochim. Acta* **1977**, *22*, 1381−1384.
(17) Shoesmith, D. W.; Sunder, S.; Bailey, M. G.; Wallace, G. J. *Corros. Sci.* **1989**, *29*, 1115−1128.
(18) Shoesmith, D. W.; Sunder, S.; Bailey, M. G.; Miller, N. H. *J. Nucl. Mater.* **1996**, *227*, 287−299.
(19) Shoesmith, D. W.; Betteridge, J. S.; Hocking, W. H. *J. Electroanal. Chem.* **1996**, *406*, 69−81.
(20) Shoesmith, D. W.; Sunder, S.; Tait, J. C. *J. Nucl. Mater.* **1998**, *257*, 89−98.
(21) Hiskey, J. B. *Inst. Min. Metall., Trans.* **1979**, *88*, c145−c152.
(22) Hiskey, J. B. *Inst. Min. Metall., Trans.* **1980**, *89*, c145−c152.
(23) Sunder, S.; Shoesmith, D. W.; Kolar, M.; Leneveu, D. M. *J. Nucl. Mater.* **1997**, *250*, 118−130.
(24) Sharma, J. N.; Bhattacharya, K.; Swami, R. G.; Tangri, S. K.; Mukherjee, T. K. *J. Radioanal. Nucl. Chem.* **1996**, *214*, 223−233.
(25) De Pablo, J.; Casas, I.; Gimenez, J.; Molera, M.; Rovira, M.; Duro, L.; Bruno, J. *Geochim. Cosmochim. Acta* **1999**, *63*, 3097−3103.
(26) Sunder, S.; Strandlund, L. K.; Shoesmith, D. W. *Electrochim. Acta* **1998**, *43*, 2359−2372.
(27) Liu, C.; Zachara, J. M.; Gorby, Y. A.; Szecsody, J. E.; Brown, C. F. *Environ. Sci. Technol.* **2001**, *35*, 1385−1393.
(28) Liu, C.; Kota, S.; Zachara, J. M.; Fredrickson, J. K.; Brinkman, C. *Environ. Sci. Technol.* **2001**, 35, 2482−2490.
(29) Wildung, R. E.; Gorby, Y. A.; Krupka, K. M.; Hess, N. J.; Li, S. W.; Plymale, A. E.; McKinley, J. P.; Fredrickson, J. K. *Appl. Environ. Microbiol.* **2000**, *66*, 2451−2460.
(30) Lloyd, J. R.; Mabbett, A. N.; Williams, D. R.; Macaskie, L. E. *Hydrometallurgy* **2001**, *59*, 327−337.
(31) Liu, C.; Gorby, Y. A.; Zachara, J. M.; Fredrickson, J. K.; Brown, C. F. *Biotechnol. Bioeng.*, submitted for publication, 2002.

Received for review July 24, 2001. Revised manuscript received December 7, 2001. Accepted December 13, 2001.

ES011159U